The Structure of Some Univalent Metal Nitrate Melts Studied by Means of Pulsed Neutron Diffraction

Toshio Yamaguchi, Yusuke Tamura, Isao Okada, and Hitoshi Ohtaki

Department of Electronic Chemistry, Tokyo Institute of Technology, Nagatsuta, Midori-ku, Yokohama 227, Japan

Masakatsu Misawa and Noboru Watanabe

National Laboratory for High Energy Physics, Oho-machi, Tsukuba-gun, Ibaraki 305, Japan

Z. Naturforsch. **40 a**, 490–496 (1985); received January 23, 1985

The structure factors of molten $LiNO_3$, $RbNO_3$ and $AgNO_3$ and the 1:1 $LiNO_3$–$RbNO_3$ mixture have been determined over a wide range of momentum transfer by neutron total scattering measurements using a pulsed spallation neutron source. Least-squares analyses applied to the intra-ionic part of the structure factors have revealed the geometry of nitrate ions to be equilateral triangular (the D_{3h} symmetry) in the melts, independent of the cations involved. The radial distribution function (RDF) of the $AgNO_3$ melt has indicated that about four nitrate ions are bound to an Ag^+ ion as a monodentate ligand with the shortest Ag–O distance of 240 pm. The contact between lithium atoms and nitrate ions was also evidenced at about 190 pm in the RDF of the melts containing lithium ions, but the orientation of the nitrate toward lithium ions was not conclusive in the present study.

Introduction

Investigations of the structure of molten univalent metal nitrates by Raman and infrared spectroscopy [1–9] have so far been focused upon the split of the ν_3 band at about 1400 cm^{-1}, which is due to the loss of degeneracy of the E mode of the NO_3 ion, i.e. the lowering symmetry from D_{3h} to C_{2v} or C_s, and upon the low-frequency bands appearing in the region of 100 to 350 cm^{-1} in molten $LiNO_3$, $AgNO_3$ and $TlNO_3$. The former characteristic of the spectra has been interpreted in terms of a specific ionic association between cations and nitrate anions [1–7, 9]. On the other hand, the low frequency bands have been ascribed to interionic interactions in quasi-crystalline aggregates from a comparison of the bands with those of the the corresponding crystal structure [1, 8, 9]. Clarke and Hartley [5], however, interpreted the spectra in terms of transient ionic associations and claimed that the low frequency Raman bands originate from localized librational modes of the nitrate ion around the C_2 axis. In an X-ray diffraction study of a series of molten univalent metal nitrates [10] it has been suggested that the nitrate ions and cations have a diamond-like arrangement in molten $NaNO_3$, KNO_3, $RbNO_3$ and $CsNO_3$ and a simple cubic arrangement in molten $AgNO_3$ and $LiNO_3$. In Time-of-Flight (TOF) neutron diffraction measurements [11], two different O–O distances within the nitrate ions were found in case of the $LiNO_3$, $AgNO_3$ and $TlNO_3$ melts and were ascribed to the C_{2v} symmetry of the nitrate ions. However, a recent X-ray diffraction study on molten $AgNO_3$ [12] has revealed that about four nitrate ions are bonded to an Ag^+ ion and hence a nitrate ion shares more than one Ag ion.

In the present study, we have performed TOF neutron diffraction measurements on molten $LiNO_3$, $RbNO_3$, $AgNO_3$ and a 1:1 mixture of $LiNO_3$–$RbNO_3$ using a pulsed spallation neutron source in order to determine the geometry of the nitrate ions in the melts and also to investigate the cation-nitrate ion interactions. The pulsed neutron source employed here is much more intense than the previous one using an electron LINAC [11], and hence a more reliable data analysis is expected.

Experimental

Neutron scattering measurements were performed with a high intensity total scattering spectrometer HIT using a pulsed spallation neutron source at

Reprint requests to Prof. Hitoshi Ohtaki, Department of Electronic Chemistry, Tokyo Institute of Technology, Nagatsuta, Midori-ku, Yokohama 227, Japan.

0340-4811 / 85 / 0500-0490 $ 01.30/0. – Please order a reprint rather than making your own copy.

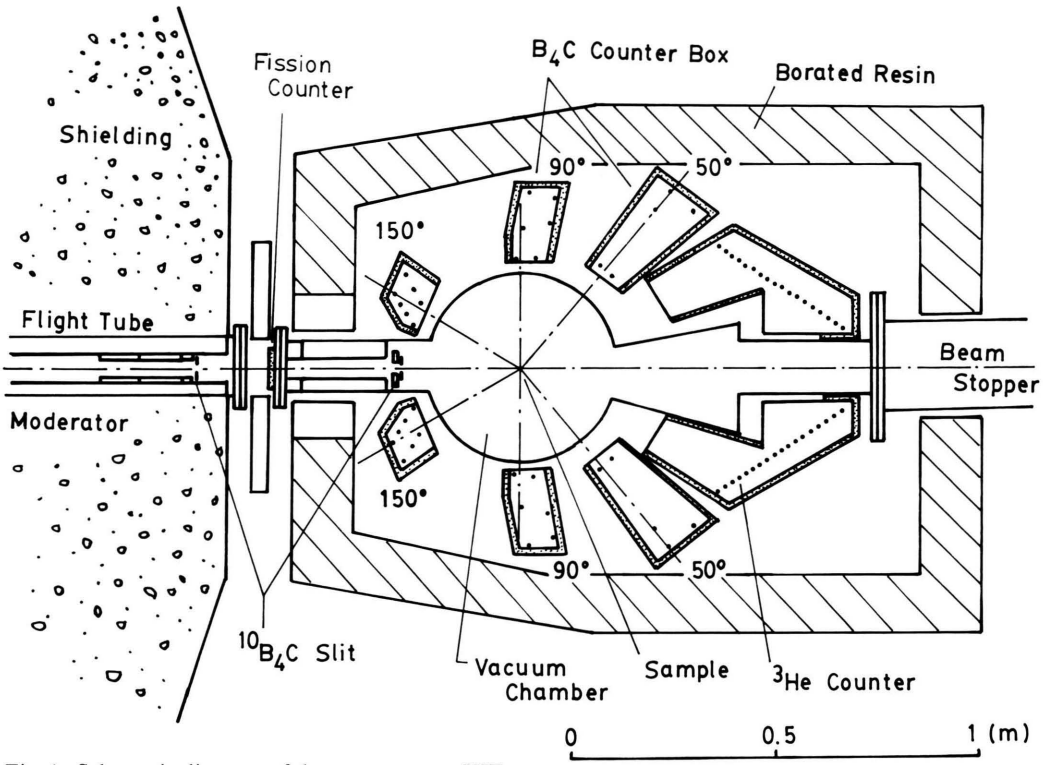

Fig. 1. Schematic diagram of the spectrometer HIT.

the National Laboratory for High Energy Physics (KEK), Tsukuba. A schematic diagram of the spectrometer is shown in Figure 1. Details of the instrument and its performance have been described elsewhere [13]. Neutron scattering data were collected simultaneously with ^3He counters at scattering angles (2θ) of 8°, 13°, 23°, 32°, 51°, 91° and 150°. At $2\theta = 91°$ and 150° counters were arranged in the geometrically focussing positions.

Metal nitrates of reagent grade were used without further purification. Powder samples of the pure salts which had been dried *in vacuo* at 100−150 °C overnight, were melted in Pyrex glass tubes with a diameter of 10 mm. The 1:1 $LiNO_3$−$RbNO_3$ mixture was melted and stirred sufficiently in a crucible before pouring it into the Pyrex tube. After cooling the melts in a desiccator the solidified metal nitrates were taken out from the tubes, transferred into quartz sample cells and sealed *in vacuo*. The sample cells have 0.4 mm wall thickness, 10 mm in inner diameter and 70 mm in height.

The samples were placed in a vacuum chamber during the measurements to prevent scattering of the incident beam by air. The sample cell was heated by two infrared lamps facing each other. The temperature of the sample was monitored by a Chromel-Alumel thermocouple and controlled within ±1 °C during the measurements. Besides the measurement of the samples, scattered intensities were measured for background, an empty cell and a vanadium rod of the same dimension as the cell. Scattering from the vanadium rod was used to normalize the measured intensities to absolute units.

The observed intensities were corrected for absorption [14], multiple [15] and incoherent scattering and the recoil effect [16].

The structure factor $S(Q)$ can be defined by

$$S(Q) = \frac{I(Q) - \sum b_i^2 + (\sum b_i)^2}{(\sum b_i)^2}, \qquad (1)$$

where $I(Q)$ represents the normalized observed intensity and b_i is the coherent scattering length of the i-th nucleus, which was taken from the literature [17]. The isotope ratio of natural Li was checked by mass spectrometry.

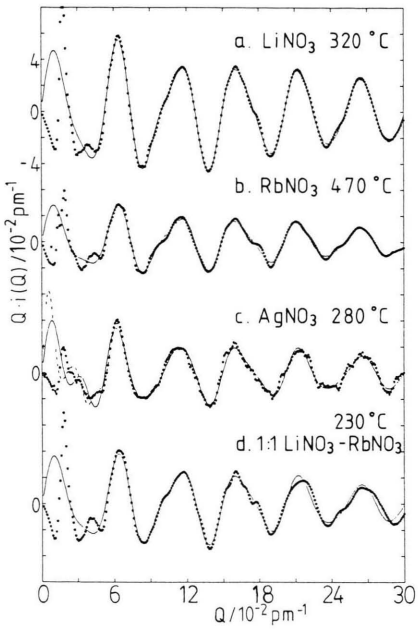

Fig. 2. Structure functions $i(Q)$ multiplied by Q of the melts (a) $LiNO_3$, (b) $RbNO_3$, (c) $AgNO_3$ and (d) 1:1 $LiNO_3$–$RbNO_3$. Dots show the experimental values and solid lines the theoretical ones for the models described in the text. The dashed line in (c) shows the theoretical values for the Ag–NO_3 orientation model (Figure 8).

The radial distribution function is calculated by the conventional Fourier transform

$$D(r) = 4\pi r^2 \varrho_0 + (2r/\pi) \int_{Q_{min}}^{Q_{max}} Q \cdot i(Q)\, M(Q) \cdot \sin(Q\, r)\, dQ\,, \qquad (2)$$

where ϱ_0 denotes the number density, Q_{min} and Q_{max} the lower and upper limits of the momentum transfer Q restricted under the experimental conditions, $M(Q)$ the modification function of the form $\sin(\pi Q/Q_{max})/(\pi Q/Q_{max})$, and $i(Q)\,(= S(Q) - 1)$ the structure function. The $i(Q)$ values multiplied by Q are shown in Figure 2.

The theoretical structure function $i(Q)_{mod}$ for a model structure of a melt is calculated according to the Debye equation

$$i(Q)_{mod} = \sum \sum n_{ij}\, b_i\, b_j\, j_0(Q\, r_{ij}) \exp(-b_{ij}\, Q^2)\,. \qquad (3)$$

Here $j_0(x)$ is a spherical Bessel function of the zeroth order, n_{ij} the number of interactions between the i-th and j-th nuclei. The temperature coefficient b_{ij} is given by $b_{ij} = \langle l_{ij}^2 \rangle / 2$, where $\langle l_{ij}^2 \rangle$ is the mean square variation of the distance between the i-th and j-th nuclei. Peak shapes for a given model are calculated by the Fourier transform of $i(Q)_{mod}$ using (2).

Results and Discussion

A) Radial distribution functions (RDFs)

The radial distribution functions for molten $LiNO_3$, $RbNO_3$, $AgNO_3$ and (1:1) $LiNO_3$–$RbNO_3$ mixture are shown in Figure 3. The first peak was observed at 125 pm for all the melts, corresponding to the expected N–O distance within a nitrate ion. The second peak appeared around 220 pm for the melts of $LiNO_3$, $RbNO_3$ and the mixture, assignable to the O–O interaction within the nitrate ion. In the RDF of the $AgNO_3$ melt the second peak was split in two, the positions of which were around 220 pm and 240 pm. In crystals of some NO_3-coordinated Ag compounds such as β-$AgNO_3$ [18], the shortest Ag–O distance has been reported to be 240–250 pm. From an X-ray diffraction study of an $AgNO_3$ melt the shortest distance between Ag^+ and the nitrate oxygen atoms has been observed at 245 pm [12]. Therefore, the peak around 240 pm was assigned to the Ag–O interaction.

In case of the $LiNO_3$ melt, the Li–O distance was expected to be about 200 pm according to the

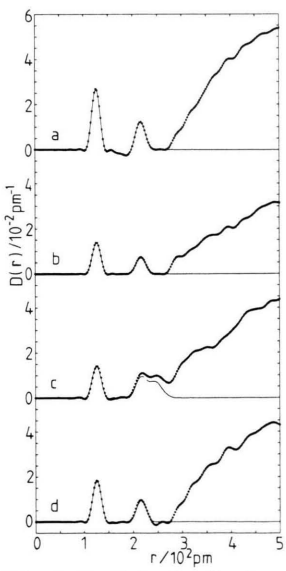

Fig. 3. Radial distribution functions of the melts: (a) $LiNO_3$, (b) $RbNO_3$, (c) $AgNO_3$ and (d) 1:1 $LiNO_3$–$RbNO_3$. Dots: experimental; solid lines: model.

sum of the effective ionic radius of Li^+ (60 pm) and the contact radius of oxygen atom (140 pm) [19]. Since the Li nucleus has a negative scattering length, the Li−O interaction should give a negative contribution to the RDF around 200 pm. In a previous neutron diffraction study [11], the asymmetric peak at 220 pm was interpreted in terms of two different O−O interactions originating from an isosceles triangular structure of the NO_3^- ion, and the contribution of the Li−O interaction was not taken into account in the analysis. However, the asymmetric feature of the peak at 220 pm can occur when the negative Li−O (200 pm) and positive O−O (220 pm) contributions to the RDF overlap. This point will be discussed in detail in the following section.

B) Structure of the NO_3^- ion

In general, short intramolecular interactions contribute to the structure factor up to high Q values while the contribution of intermolecular interactions diminishes rapidly with increasing Q. In the present study, therefore, the structure of the nitrate ion was determined by a least-squares fitting procedure applied to the $Q \cdot i(Q)$ values in the high Q region except for the $RbNO_3$. The function $U = \sum Q^2 [i(Q)_{obs} - i(Q)_{mod}]^2$ was minimized with the distance r_{ij}, the temperature coefficient b_{ij} and the number of interactions n_{ij} in (3) as optimizing parameters.

In case of the $RbNO_3$ melt another fitting procedure was used. As is seen in the RDF of the $RbNO_3$ melt (Fig. 3b), the peaks originating from the intra-ionic N−O and O−O interactions within the nitrate ion are well separated from the intermolecular interactions appearing at $r > 290$ pm. Thus, the experimental intra-ionic structure function $Q \cdot i(Q)_{intra}$ can be obtained by a reverse Fourier transform according to

$$i(Q)_{intra} = \int_{r_{min}}^{r_{max}} D(r) \sin(Q r)/(Q r)\, dr . \qquad (4)$$

Here, r_{min} and r_{max} are the lower and upper limits of the r-range within which peaks of interest fall; in the present case they were set to be 0 and 260 pm, respectively.

Figure 4 (dots) shows the $Q \cdot i(Q)_{intra}$ values thus obtained, for which the least-squares fits were carried out in the whole Q region. The distance and the

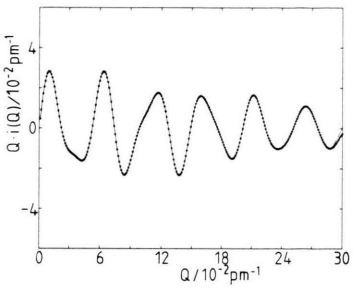

Fig. 4. Experimental intra-ionic part of the structure function of the $RbNO_3$ melt obtained by (4) (dots) and calculated from the least-squares fit (line).

temperature coefficient of the N−O and O−O pairs within the nitrate ion were varied independently. The final results are given in Table 1. The values obtained in the present investigation are in good agreement with those reported in a previous study [11]. The nitrate ion has a D_{3h} symmetry structure in the $RbNO_3$ melt. The model reproduces the observed values well as shown in Figures 2−4.

In case of the molten $LiNO_3$, $AgNO_3$ and $LiNO_3$−$RbNO_3$ mixture, the contribution from the short Li−O (200 pm) and Ag−O (240 pm) interactions discussed in the previous section should be carefully checked over the Q-range employed in the refinements since their contribution to the total structure function might still remain in a moderate Q region.

In order to estimate the contribution of the shortest Ag−O interactions, we analysed the peak at 240 pm by assuming a Gaussian shape. The result indicated that the frequency factor of the Ag−O contacts was about four with $r_{Ag-O} = 243$ pm and $b_{Ag-O} = 100$ pm^2. The theoretical $Q \cdot i(Q)$ values of the Ag−O interaction thus estimated are drawn in Fig. 5d, together with those of the N−O and O−O interactions (Figures 5a−c). Figure 5d clearly shows that the Ag−O contribution is significant up to 0.2 pm^{-1}, but negligible at $Q > 0.2$ pm^{-1}. Therefore, the structure of nitrate ion in the $AgNO_3$ melt was determined by the least-squares fits in the Q-range of 0.2−0.3 pm^{-1}. In order to examine the symmetry of the nitrate ion, the following two models were tested.

Model A: Nitrate ion with D_{3h} symmetry. The distances and the temperature coefficients of the N−O and O−O atom pairs were allowed to vary independently.

Table 1. Results of the least-squares fits with the distance r (pm), the temperature coefficient b (pm^2), the number of interactions n, and the agreement factor R defined in the text. The estimated standard deviations are given in parentheses. The values in brackets are those reported by Suzuki and Fukushima [11] (* Fixed).

Melts		Range of $Q/10^{-2}$ pm^{-1}	N–O			O–O or O′–O′			O–O′			M–O			
			r	b	n	r	b	n	r	b	n	r	b	n	R
$LiNO_3$	A	15–30	125.0 (1)	8 (1)	3	215.5 (4)	29 (2)	3							0.09
	B	15–30	125.1 (1)	8 (1)	3	209 (1)	10 (10)	1	219.6 (1)	10	2				0.14
		5–20	125.0*	8*	3	215.5*	29*	3				189 (2)	16 (5)	3.2 (9)	0.08
		[9–20	126	14	3	209	25	1	221	25	2]				
$RbNO_3$		0.1–30	125.5 (1)	11 (1)	3	216.1 (3)	25 (2)	3							0.03
		[9–20	125	10	3	217	27	3]							
$AgNO_3$	A	20–30	124.9 (1)	10 (1)	3	214.9 (5)	19 (2)	3							0.26
	B	20–30	125.5 (1)	10 (1)	3	211 (1)	10 (10)	1	220.5 (5)	10	2				0.36
		5–20	124.9*	10*	3	214.9*	19*	3				242 (2)	90 (10)	4.3 (5)	0.17
		[9–20	127	16	3	210	25	1	222	25	2]				
(1:1) $LiNO_3$–$RbNO_3$		5–30	124.9 (1)	12 (3)	3	216.7 (2)	32 (2)	3				193 (2)	30 (20)	4 (1)	0.18

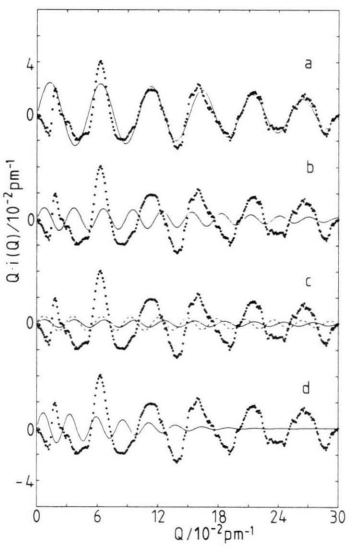

Fig. 5. Comparison of the pair structure functions for the $AgNO_3$ melt (a) $3\times$N–O, (b) $3\times$O–O from D_{3h}, (c) $2\times$O–O′ (– – –), $1\times$O′–O′ (——) from C_{2v} and (d) $4\times$Ag–O, together with the observed ones (dots).

Model B: Nitrate ion with C_{2v} symmetry having two different O–O distances ($2\times$O–O′, $1\times$O′–O′) with the same temperature coefficient. r_{N-O}, b_{N-O}, $r_{O-O'}$, $r_{O'-O'}$ and $b_{O-O'}$ ($= b_{O'-O'}$) were treated as independent parameters. The values reported in [11] were taken as initial values.

The usual agreement factor R defined by

$$R^2 = \Sigma Q^2 [i(Q)_{exp} - i(Q)_{mod}]^2 / \Sigma Q^2 i(Q)^2_{exp} \qquad (5)$$

was used to choose the most likely model.

The final results are summarized in Table 1.

The R-value for the D_{3h} model was significantly smaller than that for the C_{2v} model, and thus it was concluded that the nitrate ion has an equilateral triangular structure in the $AgNO_3$ melt.

The data for the molten $LiNO_3$ and $LiNO_3$–$RbNO_3$ mixture were analysed in a similar manner as for the $AgNO_3$ melt. Since the scattering length of the Li atom is about one-third of that of the Ag atom, the frequency factor of Li–O pairs was difficult to be estimated from the RDF. Thus the Li–O interaction was assumed to have $n_{Li-O} = 4$ and $r_{Li-O} = 200$ pm according to the literature [19] and its contribution was compared with those from the N–O and O–O interactions. The result showed that the oscillation of the short Li–O interaction diminishes around 0.12 pm^{-1}. Thus the least-squares fits were performed in the Q-range of 0.15–0.30 pm^{-1} for the two models. The results are given in Table 1. Judging from the R-value, the D_{3h} symmetry model was again preferred in the $LiNO_3$ melt.

This conclusion held also for the $LiNO_3$–$RbNO_3$ mixed melt although the Li–O contribution was small in the RDF. The final parameter values from the least-squares fits are given in Table 1.

The present conclusion that nitrate ions have a structure of the D_{3h} symmetry in the $AgNO_3$ and $LiNO_3$ melts differs from that given in [11]. This is probably because the significant Li–O and Ag–O interactions were not taken into account in the analyses performed in [11]. It should be borne in

mind that the D_{3h} symmetry structure for nitrate ion concluded in the present study is both time- and space-averaged. From a dynamical point of view, the structural distortion of the nitrate ion indicated in the spectroscopic studies [1–9] may be discussed on the basis of frequency shifts in spectra. However, if the triangular structure of NO_3^- could significantly deform so as to be isosceles triangular, the temperature coefficients of the N–O and O–O interactions within the NO_3^- ion should be very large. The *b* values in Table 1, however, show that this is not the case in the melts and hence a significant deformation of the triangular structure of NO_3^- ion may not be expected in these melts. It should be noted that a recent depolarized Rayleigh spectrum of molten lithium nitrate has supported the D_{3h} symmetry of the nitrate ion in the melt [20].

C) Cation – nitrate ion interaction

In the previous section the $M^+-NO_3^-$ interaction has been discussed for molten $AgNO_3$. The structure parameters of the Ag–O interactions were determined by least-squares fits in the Q region of $0.05-0.20\ pm^{-1}$, in which there is a significant Ag–O contribution in the experimental structure function (Figure 5). During the calculations, the parameters of the N–O and O–O pairs within the nitrate ion were fixed to the values obtained in the previous section to decrease the number of independent parameters varied simultaneously. The final results given in Table 1 show that about four nitrate oxygen atoms coordinate to an Ag^+ ion with an Ag–O distance of 242 pm. The peak shape of each atom pair is demonstrated in Figure 6. The agreement between the experimental and calculated $Q \cdot i(Q)$ and $D(r)$ functions is shown in Figs. 2c and 3c, respectively.

In order to determine the number of oxygen atoms around Li^+, similar calculations were carried out in the Q range $0.05-0.20\ pm^{-1}$ for the structure functions of molten $LiNO_3$ and the $LiNO_3-RbNO_3$ mixture. The final results are summarized in Table 1, showing that the number of Li–O contacts at 190 pm should be 3–4 in the melts. The peak shapes of the N–O, O–O and Li–O interactions are reproduced in Figure 7.

The present result that more than one nitrate ion coordinates to an Ag^+ and an Li^+ ion implies that nitrate ions must be shared by some of the cations.

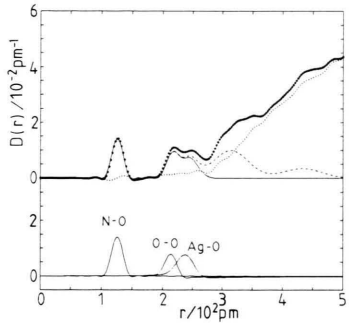

Fig. 6. The peak shapes of the N–O, O–O and Ag–O interactions for the $AgNO_3$ melt (below). Their sum is shown by the solid line (above), together with the experimental values (circles). The dashed line shows the calculated values based on the orientation model (Fig. 8). The difference between the experimental and the calculated values is represented by the dots.

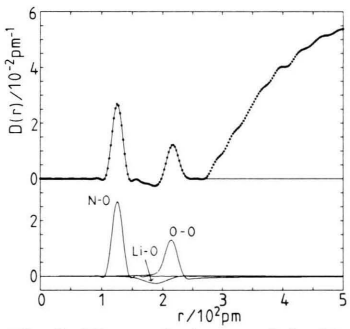

Fig. 7. The peak shapes of the N–O, O–O and Li–O interactions (below) and their sum (solid line, above), together with the experimental values (dots).

In this situation, various instantaneous geometries of the NO_3^- ions may exist in the system and the time-averaged structure of the various instantaneous distortions of the nitrate ions is of D_{3h} symmetry as is detected by the present diffraction method.

The broad peaks around 290–320 pm and 400–500 pm in the RDF of the $AgNO_3$ melt (Fig. 3) indicate the presence of long-range orientations in $Ag^+-NO_3^-$ interactions. No such peak was observed in the corresponding RDFs of the other melts. In an X-ray diffraction study of an $AgNO_3$ melt, Holmberg and Johansson [12] have proposed a model for an $Ag-NO_3$ orientation illustrated in Fig. 8, similar to that found in the structure of β-$AgNO_3$ crystals [18]. The peak shape calculated from this model with parameter values given in Table 2 is drawn in Fig. 6 by a dashed line, which corresponds well to the broad peaks at 290–320 pm and 400–500 pm

Table 2. Parameters used for the model calculation of $Ag-NO_3$ orientation illustrated in Fig. 8; interatomic distance r in pm, temperature coefficient b in pm^2 and number of interactions n per Ag atom.

	r	$b/10$	n
Ag–N	315	40	4.3
Ag–O1	242	9	4.3
Ag–O2	307	40	4.3
Ag–O3	435	60	4.3

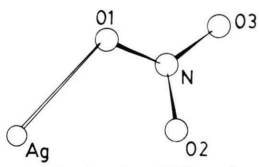

Fig. 8. An $Ag-NO_3$ orientation model [12].

in the RDF of the $AgNO_3$ melt. Thus about four nitrate ions are likely to coordinate to Ag^+ as a monodentate ligand.

In the melts of $LiNO_3$, $RbNO_3$ and $LiNO_3$–$RbNO_3$ mixture, the orientation of the nitrate ions toward the cations was not concluded from the present diffraction data since longer M–N and M–O peaks within the $M-NO_3$ interaction were not clearly resolved in the RDFs. However, molecular dynamics (MD) calculations of the same systems have indicated that Li and Rb atoms do not have any specific orientation toward NO_3 ion [21, 22]. These results from the MD method are consistent with the non-appearance of a specific peak in the r-range of 290–400 pm of the RDFs of molten $LiNO_3$, $RbNO_3$ and 1:1 $LiNO_3$–$RbNO_3$ mixture (Figure 3).

Concerning the coordination number n_{ij} of the cation – nitrate interactions, the MD calculations have revealed various coordination numbers around Li and Rb atoms [21, 22]. Thus, the values obtained from the present diffraction method should be taken as an averaged one of various numbers of the nearest neighbors in the melts.

Acknowledgements

We wish to thank the members of the HIT group for assistance during measurements. A part of the calculations was carried out at the Institute for Molecular Science (Okazaki) and at the National Laboratory for High Energy Physics (Tsukuba). The present work has been supported by the Grant-in-Aid for Scientific Research for the Ministry of Education, Science and Culture (No. 58740274).

[1] J. K. Wilmshurst and S. Senderoff, J. Chem. Phys. **35,** 1078 (1961).
[2] G. E. Walrafen and D. E. Irish, J. Chem. Phys. **40,** 911 (1964).
[3] S. C. Wait and A. T. Ward, J. Chem. Phys. **44,** 448 (1966).
[4] C. A. Angell, J. Wong, and W. F. Edgell, J. Chem. Phys. **51,** 4519 (1969).
[5] J. H. R. Clarke and P. J. Hartley, J. Chem. Soc. Faraday Trans. II, **68,** 1634 (1972).
[6] (a) G. J. Janz and D. W. James, J. Chem. Phys. **35,** 739 (1961); (b) G. J. Janz and T. R. Kozlowski, J. Chem. Phys. **40,** 1699 (1964); (c) S. C. Wait, Jr., A. T. Ward, and G. J. Janz, J. Chem. Phys. **45,** 133 (1966); (d) E. Eluard, K. Balasubrahmanyam, and G. J. Janz, J. Chem. Phys. **59,** 2756 (1973).
[7] (a) J. P. Devlin, K. Williamson, and G. Austin, J. Chem. Phys. **44,** 2203 (1966); (b) P. Li and J. P. Devlin, J. Chem. Phys. **49,** 1441 (1968); (c) J. P. Devlin, G. Ritzhaupt, and T. Hudson, J. Chem. Phys. **58,** 817 (1972).
[8] (a) D. W. James and W. H. Leong, J. Chem. Phys. **51,** 646 (1969); (b) D. W. James and W. H. Leong, J. Chem. Soc. Faraday Trans. II, **66,** 1948 (1970).
[9] C. H. Huang and M. H. Brooker, Spectrochim. Acta **32 A,** 1715 (1976).
[10] H. Ohno and K. Furukawa, J. Chem. Soc. Faraday Trans. I, **74,** 297 (1978).
[11] K. Suzuki and Y. Fukushima, Z. Naturforsch. **32 A,** 1438 (1977).
[12] B. Holmberg and G. Johansson, Acta Chem. Scand. **A 37,** 367 (1983).
[13] Y. Ishikawa, N. Watanabe, Y. Endoh, N. Niimura, and J. M. Newsome, Ed., Proceedings of the Fourth Meeting of International Collaboration on Advanced Neutron Source (ICANS-IV), KEK-Report II, KEK, Tsukuba, 1981.
[14] H. H. Paalman and C. J. Pings, J. Appl. Phys. **33,** 2635 (1962).
[15] I. A. Blech and B. L. Averbach, Phys. Rev. **A 137,** 1113 (1965).
[16] K. Suzuki, M. Misawa, K. Kai, and N. Watanabe, Nucl. Inst. Method **147,** 519 (1977).
[17] Neutron Diffraction Newsletter, M. S. Lehmann, Ed., The Neutron Diffraction Commission, 1982.
[18] P. Meyer, A. Rimsky, and R. Chevalier, Acta Crystallogr. **B 32,** 1143 (1976).
[19] R. D. Shannon, Acta Crystallogr. **A 32,** 751 (1976).
[20] R. Martin and R. Romanetti, Abstracts of Euchem Conference on Molten Salts, Elsinore, Denmark, 1984.
[21] M. Mikami, I. Okada, T. Yamaguchi, H. Ohtaki, and K. Kawamura, Proceedings of the First International Symposium on Molten Salt Chemistry and Technology, Kyoto, 1983.
[22] I. Okada, T. Yamaguchi, and H. Ohtaki, Abstracts of Euchem Conference on Molten Salts, Elsinore, Denmark, 1984.